Journal of Engineering Sciences
Assiut University
Faculty of Engineering
Vol. 48
No. 2
March 2020
PP. 200–211

DETECTING LAND COVER CHANGES USING VHR SATELLITE IMAGES: A COMPARATIVE STUDY

Farrag A. Farrag [1], Yasser G. Mostafa [2], Nasser A. Mohamed [3]

[1] *Civil Eng. Dpt. Faculty of Engineering, Assiut University.*
[2, 3] *Civil Eng. Dpt. Faculty of Engineering, Sohag University.*

Received 10 October 2019; Accepted 24 October 2019

ABSTRACT

The new satellites sensors such as GeoEye , WorldView and Ikonos , provide new data for better delineation, detection, and visualization of Land cover changes. Several techniques have been proposed and developed for change detection automatically. The main aim of this research is to assess the use of very high-resolution satellites images in monitoring land cover changes in Egypt.

Five change detection techniques have been tested using Ikonos and WorldView images. The techniques considered are image difference, image ratio, principal component analysis, post-classification comparison, and multi-date direct classification. The accuracy of each technique is evaluated via the overall accuracy and kappa coefficient. The results showed that the principal component analysis technique produced more accurate change detection map compared to other methods. Also, it was found that changes from vegetation to urban in the study area are greater than changes from bare soil to vegetation.

Keywords: change detection, very high-resolution, object-based.

1. Introduction

Change Detection (CD) is the process of distinguishing differences between two sets of images taken at different times for the same area. Land cover change detection from Very High-Resolution (VHR) images is considered one of the most challenging issues in remote sensing. Change detection methods have known a strong improvement with the availability of (VHR) images. Numerous techniques in CD are being proposed which provide a great significance in the field of land cover and land use environment assessment, urban expansion monitoring, managing natural resources, and rapid evaluation of disaster events [1].

The techniques of change detection can be divided into two groups, pixel-based and object-based. In the first group, the changes between the two images are compared for each pixel independently. In the second group, the images are segmented into disjoint and homogeneous objects, then changed features are extracted and compared [2]. Several

* Corresponding author.
E-mail address: *naserahmed@eng.sohag.edu.eg*

change detection reviews for pixel-based analysis have been published [3, 4, 5, 6] which summarized and categorized CD techniques based on different viewpoints.

Tewkesbury et al [6] grouped change detection techniques into six categories, including layer arithmetic, change vector analysis, post-classification change, direct classification, transformation, and hybrid change detection. Coppin et al [7] mentioned that change detection techniques can be classified into nine different categories. They are post-classification comparisons, univariate image differencing, composite analysis, image ratio, change vectors analysis, bi-temporal linear data transformation, image regression, multi-dimensional temporal feature space analysis, multi-temporal spectral mixture analysis, plus the hybrid methods.

Object-Based Change Detection (OBCD) provides a significant improvement in different application areas related to multi-temporal remote sensing images, especially for VHR images [8]. Zhang et al [9] classified OBCD methods into three groups: class-object-based, image-object-based, and multitemporal-object-based.

Hussain et al [10] grouped object-based change detection methods into three groups, including classified object change detection, direct object change detection and multitemporal object change detection. The object-based imaged analysis methods have been considered more appropriate for VHR satellite image data and change detection reviews based on object-based analysis can be found in [11, 12]

In this paper, the images are corrected geometrically and shadow restoration was applied to the produced corrected images. Then, a comparison between five well-known change detection methods was performed to find the most suitable method that can be used in the Egyptian environment. The rest of this paper is organized in the following sections. The Study area and data used are illustrated in Section 2. Data preprocessing are depicted in section 3. Change detection techniques are discussed in section 4. Section 5 illustrates the quantitative analysis of the result. Conclusions are given in Section 6.

2. Study area and data used

The study area lies in Assiut City, the capital of Assiut Governorate (figure 1) which is one of the ancient capitals of Egypt. It has a geographical extent of 26º 40` N to 27º 30` N and 30º 41` E to 31º 31` E. Assiut city is considered one of the fastest growing urban areas in Egypt. Two very high-resolution images were used in this study from IKONOS-2 satellite (Figure 1-a) and WorldView-2 satellite (Figure 1-b). IKONOS image was captured on 17th February 2006 while WorldView image was acquired on 4th March 2016. Table 1 shows the characteristics of the two images.

Table 1.
Characteristics of IKONOS-2 and WorldView images.

	IKONOS-2		WorldView-2	
Band	Wave length (µm)	Resolution (m)	Wave length (µm)	Resolution(m)
coastal blue	----	----	400-450	1.84
blue	450-530	4	450-510	1.84
green	520-610	4	510-580	1.84
yellow	----	----	585-625	1.84
red	640-720	4	630-690	1.84
red edge	----	----	705-745	1.84
near-IR1	760-860	4	770-895	1.84
near-IR2	----	----	860-1040	1.84
Pan	450-900	1	450-800	0.46

(a) (b)

Fig. 1. Image of Assiut city and its surroundings (a) The IKONOS-2 image of 2006 and (b) The WorldView-2 image of 2016.

3. Data preprocessing

In order to present the satellite images in a more appropriate form for better interpretation and extracting the maximum information, two stages were performed; image geo-referencing and shadow restoration.

3.1. Image geo-referencing

Image registration is to geometrically match one image to another image that have been taken from different viewpoints at different times or by different sensors. It is an important image processing stage [13]. In this paper, IKONOS-2 image of 2006 was geometrically corrected to Egyptian Transverse Mercator (ETM). The WorldView-2 image of 2016 was corrected through IKONOS-2 image of 2006 and resampling process was carried out using the nearest neighbor approach.

3.2. Shadow restoration

Shadow is considered as one of the main obstacles in satellite images which reduce the accuracy of change detection and information extraction [14]. Shadow restoration is a significant step to remove or reduce the effect of shadow. Shadow restoration procedure consists of two major steps; detection and compensation

3.2.1. Shadow detection

In this study shadow detector index (*SDI*) proposed by Mostafa and Abdelhafiz [15] was used. For each image pixel, *SDI* index is calculated using the following formula:

$$SDI = \left(\frac{(1 - PC_1) + 1}{((G - B) * R) + 1} \right) \tag{1}$$

Where PC_1, *R*, *G*, and *B* are normalized components of the first principal component, red band, green band, and blue band respectively.

High values of the shaded regions are obtained in the index histogram. Image thresholding is carried out to detect shadow area.

3.2.2. Shadow compensation

Despite the reflectance that have been in shadow areas are weak, there is still beneficial information which makes shadow restoration possible [16]. Shadow areas can be enhanced using the surrounding information of shadow [17]. In this work, Linear Correlation Correction (LCC) technique is selected for shadow restoration. In the LCC method, brightness of shadows can be restored by a linear relationship as follows:

$$DNn = \left(\frac{\sigma_{non-shadow}}{\sigma_{shadow}} \right) \left(DN_{shadow} - \mu_{shadow} \right) + \mu_{non-shadow} \quad (2)$$

where *DNn* is the digital number of the corrected image. σ_{shadow} and $\sigma_{\text{non-shadow}}$ are the standard deviation of the shadow and non-shadow image respectively. μ_{shadow} and $\mu_{\text{non-shadow}}$ are the mean of shadow and non-shadow image respectively. DN_{shadow} is the digital number of the shadow image.

This step was applied for IKONOS-2 image of 2006 and WorldView-2 image of 2016 using model maker in ERDAS IMAGEN 2013.

4. Change detection techniques

Change detection techniques can be divided to two categories, pre-classification and post-classification. In first technique change map is created from multitemporal data, then classify change maps [18]. Three Pre-classification methods are tested in this paper; principal component analysis, image differencing and image ratioing. In addition, two post-classification methods are used; Post-Classification Comparison (PCC), and Multi-date Direct Classification (MDC). The eCgnition developer and ERDAS IMAGEN 2013 software were used in this study.

4.1. Image differencing (ID)

In image differencing technique, pixel values in the first image is subtracted from the corresponding pixel in the second image. Residual image produced represents the changes that had occurred between the two dates. The subtraction results in positive and negative values in areas of surface change and zero values in areas of no change [4]. The image differencing method can be applied to a single band or to multiple bands. The approach itself can be used for the object-oriented image differencing [19]. The mean value of each object in the first image is subtracted from the corresponding object in the second image.

$$I_d(i,j) = I_1(i,j) - I_2(i,j) \quad (3)$$

where I_d is the difference image, (i,j) are image coordinates, I_1 and I_2 are images for first and second time respectively.

In order to apply this method, the separate images are stacked in a multitemporal composite image. Then the stacked image was segmented using Multiresolution segmentation algorithm with scale parameter 80. Band 1 [blue], band 2 [green], band 3 [red], and Band 4 [NIR] in IKONOS-2 image of 2006 were subtracted from Band 2 [blue], band 3[green], band 5 [red], and Band 7 [NIR] in WorldView image of 2016.

After that, training data have been selected from various areas on the change image resulted to represent the change categories. For each category a number (5-10 at a minimum) of training areas have been selected to ensure that the spectral properties of each class are represented[20] . The change image was classified using Nearest Neighbor Classifier (NN) into six classes; No Change (NC), Vegetation to Urban (V-U), Vegetation to Bare soil (V- B), Vegetation to Water (V-W), Water to Urban (W-U), and Bare soil to Vegetation (B-V) as shown in Fig. 2.

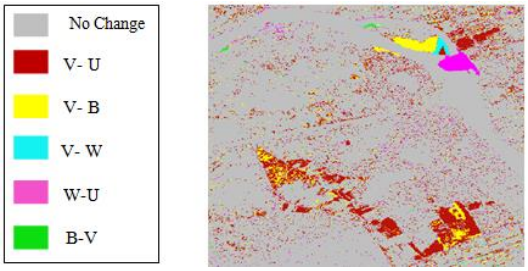

Fig. 2. The change map of image differencing technique with nearest neighbor classifier.

4.2. Image ratioing (IR)

In image ratioing technique, two co-registered image dates are rationed object by object in each band. The ratio values near to one refer to no-change area, while changed area will have higher or lower values [21]. A ratio between two co-registered images is computed as follows:

$$Ir\ (i,j) = I_1(i,j) / I_2(i,j) \quad (4)$$

where Ir is the ratio image, (i,j) are image coordinates, I_1, I_2 are images for first time and second time respectively.

In this technique, the separated images are combined into a multitemporal composite image, and then the stacked image was segmented. One band of the WorldView image of 2016 was rationed to its corresponding band in the IKONOS-2 image of 2006. Change map of image ratioing technique (Fig. 3) was produced by the nearest neighbor classification.

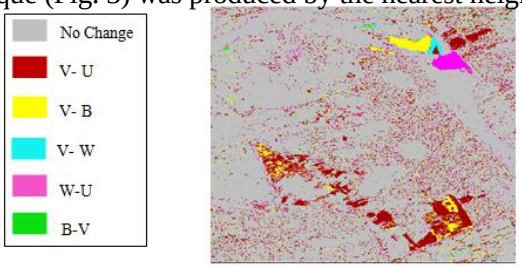

Fig. 3. The change map of image ratioing technique with nearest neighbor classifier.

4.3. Principal component analysis (PCA)

There are two techniques for PCA to detect the changes in remotely sensed imagery. The first one is to transform each image that was taken at various dates into a new PCs image. After that, bands that have been selected from new images are compared with each other using other techniques of change-detection like image ratioing. In the second technique images that were taken in various dates are combined into new one image. Then the combined bands are transformed into PCs. Accordingly, there will be a high correlation between two images of the non-changed areas, and a relatively low correlation between the significantly changed areas. Most change information can be found in the first four components [22]. In this paper, the second technique has been applied.

The four bands from the IKONOS-2 image of 2006 were combined to eight bands from the WorldView image of 2016 to build a new twelve band image. Farrag and Mostafa [23] Used PC1, PC1&PC2, PC1to PC3, and PC1to PC4 for change detection. They found that the first four components have the most information of data so that PC1to PC4 were used for supervised classification using the pixel-based method.

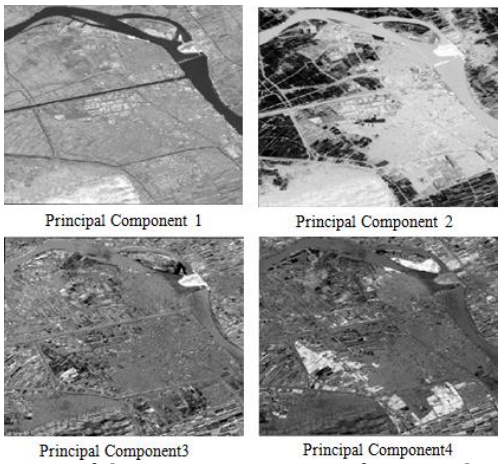

Fig. 4. The principal components of the IKONOS-2 image of 2006 and WorldView image of 2016.

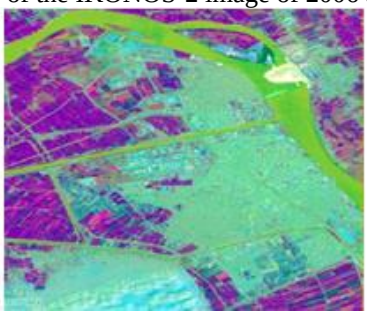

Fig. 5. Principal components composite image of IKONOS-2 image of 2006 and WorldView image of 2016, PC3 = red, PC2 = green and PC1= blue.

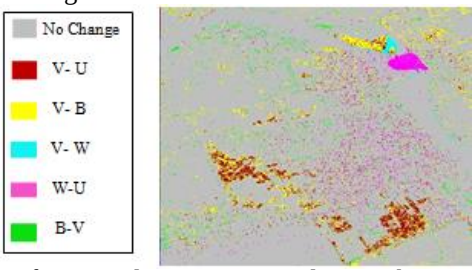

Fig. 6. The change map of Principal component analysis technique with maximum likelihood classification.

4.4. Post-classification comparison (PCC)

Post-classification comparison technique makes a logical comparison between two independent classified maps. Different methods of classification can be used according to image characteristics. PCC generates a detailed matrix of "from-to" change [1], which provide direct information on the nature of changes of land cover. The accuracy of PCC depends on the precision of the geometric registration of the two images and their classification. In this method, each image was classified individually, and then the classified images were compared.

4.4.1. Post classification comparison pixel-based

In this method, training areas of different land cover types were selected and supervised classification was carried out with five different methods; Maximum Likelihood, Spectral Correlation Mapper, Minimum Distance, Spectral Angle Mapper, and Mahalanobis

Distance. Maximum Likelihood classification has higher overall accuracy than the other methods (table 2). Fig. 7 and Fig. 8 show the results of maximum likelihood classification for IKONOS-2 image of 2006 and WorldView image of 2016 respectively.

Table 2.
Evaluation of image classification.

Classification method	IKONOS-2		WorldView-2	
	Overall accuracy	kappa coefficient	Overall accuracy	kappa coefficient
Maximum Likelihood	75.12%	0.69	81.71%	0.7
Spectral Correlation Mapper	51.43%	0.43	61.92%	0.57
Minimum Distance	51.30%	0.43	73.21%	0.67
Spectral Angle Mapper	53.24%	0.45	65.54%	0.61
Mahalanobis Distance	55.96%	0.44	69.58%	0.62

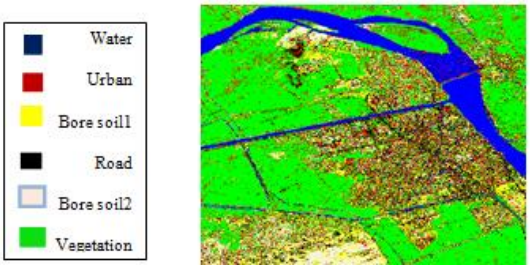

Fig. 7. Classification of IKONOS-2 image with maximum likelihood method.

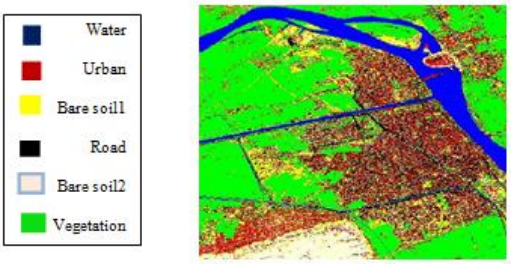

Fig. 8. Classification of WorldView image with maximum likelihood method.

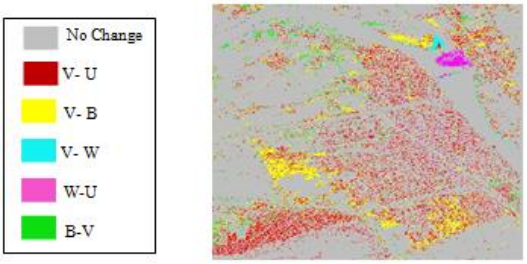

Fig. 9. The change map of Post classification comparison [pixel-based] technique

4.4.2. Post classification comparison object-based

In the PCC object-based method, each image was segmented separately using multiresolution segmentation with scale parameter 80 and training areas were selected. After that nearest neighbor classification was applied to IKONOS-2 image of 2006 and WorldView image of 2016 (Fig. 10 and Fig. 11 respectively). Results showed that this method has very good overall accuracy and Kappa for WorldView image of 2016 (89.8% and 0.87 respectively) and for IKONOS-2 image of 2006 (85.61% and 0.82 respectively).

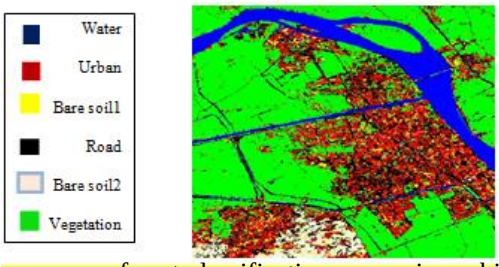

Fig. 12. The change map of post-classification comparison object-based technique.

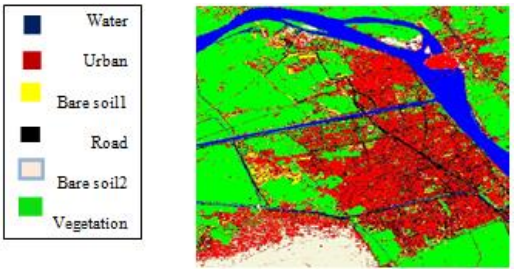

Fig. 11. Classification of WorldView image with nearest neighbor method.

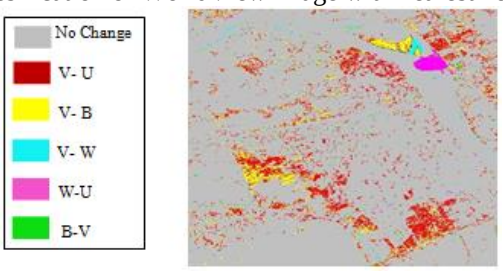

Fig. 10. Classification of IKONOS-2 image with nearest neighbor method.

4.5. Multi-date direct classification (MDC)

In this method, multi-temporal images were stacked together and classified. Then, change detection was determined by considering each change as a class. Classification process is used to distinguish all classes and all transitions.

IKONOS-2 image of 2006 and WorldView image of 2016 are combined into one multitemporal image (Fig. 13) using ERDAS IMAGEN 2013. Change detection is carried out (Fig. 14) considering each transition as a class. The classifier is trained to recognize all classes and transitions using eCgnition developer software.

Fig. 13. Composite image IKONOS-2 image and WorldView image (12 bands).

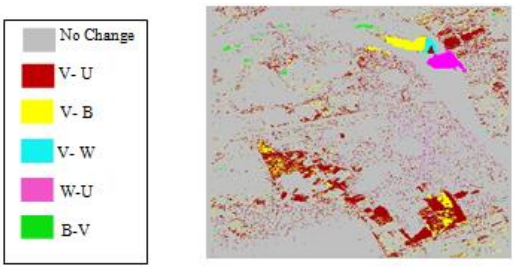

Fig. 14. The change map of direct multidate classification technique.

4.6. Classification accuracy assessment

Accuracy assessment was applied (overall accuracy and kappa coefficient) to evaluate the accuracy of each method. The number of samples of the reference data is determined to be at least 50 samples per class included in the error matrix. Samples number for each category might be adjusted based on the relative importance of that category for a particular application. The study area contains six change classes, so 50x6= 300 samples can be considered. To satisfy the importance and variability within each category 367 samples were added over 300 samples to be 667 samples (distributed as 394 for NC, 65 for V-U, 54 for V-B, 51 for V-W, 52 for W-U, and 51 for B-V). The overall accuracy of different change detection techniques and producer's accuracy are given in Table 3. Fig 15 shows overall accuracy for different change detection techniques that have been used in this research.

Table 3.
Overall accuracy of change detection techniques.

Method	Producer's Accuracy	User's Accuracy	Kappa coefficient	Overall Accuracy
ID	84.1%	81.76%	0.79	86.77%
IR	79.43%	83.42%	0.75	84.66%
PCA	94.95%	87.61%	0.89	92.24%
PCC-pixel	64.56%	68.51%	0.59	74.25%
PCC-object	75.72%	79.83%	0.72	83.25%
DMC	79.72%	80.92%	0.75	84.48%

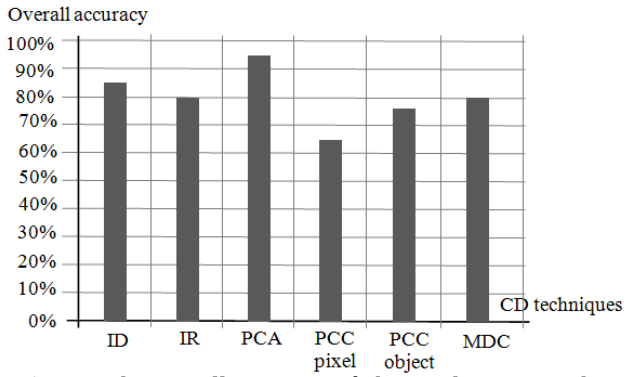

Fig. 15. The overall accuracy of change detection techniques.

5. Quantitative analysis of the result

Results in image differencing technique (Fig. 2) showed some misclassification in the classes of V-B which appear in the lower right of the study area and the class B-V which appear in the upper left. In image ratioing technique some misclassification in the classes of B-V which appears in the upper left of the study area and class V-B which appears in the lower right (Fig. 3).

The change map for principal component analysis technique (Fig. 6) was classified by using maximum likelihood classification. This method showed some misclassification in the classes of V-U which appear in the lower right and the left of the study area. In PCC, object-based technique has higher overall accuracy than the pixel-based. The object-based change detection techniques are considered more suitable for VHR image data. The results of Multi-date Direct Classification technique (MDC) method showed that the direct multidate classification technique has a more overall accuracy than PCC. This method showed misclassification in the class of (B-V), and it has a better overall accuracy of the final change map (Fig. 14).

By comparing the change detection methods, the highest accuracy was obtained by using the principal component analysis (92.24%) and low accuracy was obtained by PCC pixel-based (74.25 %). The quantitative analysis was carried out on the resulting image of the principal component analysis. The area of each class was calculated and given in Table 4. Most of the change of vegetation to bare soil, vegetation to water, and water to urban are located in the New Assiut Barrage project and its hydraulic power plant in the east north of the study area. The highest percentage of change was found in class vegetation to urban (2.86 %). Most of the changes from vegetation to urban are caused by new settlement and the growth in the urban area over the adjacent vegetation area. The growth of cities and villages in Egypt must be monitored almost annually to prevent the illegal construction of buildings.

Table 4.
Result of change classes that occurred between IKONOS-2 image of 2006 and WorldView image of 2016 in Assiut city and surrounding.

Class	Area in Km^2	% Of Total Study Area
No Change	38.76	94.55%
V- U	1.17	2.86%
V- B	0.6	1.46%
V- W	0.063	0.15%
W-U	0.27	0.66%
B-V	0.13	0.31%
Total	41	100%

6. Conclusions

This work aims to find the most suitable technique for change detection using VHR satellite images that can be applied to the Egyptian environment. The change detection techniques that have been evaluated are image differencing, image ratio, principal component analysis, post-classification comparison, and multi-date direct classification. The highest accuracy was obtained by using the principal component analysis (92.24%). Low accuracy was obtained by post-classification comparison with pixel-based (74.25 %). The highest percentage of change was in class vegetation to urban (2.86 %) and class vegetation to bare soil (1.46 %) which located at the west and south of the study area.

Vegetation areas changed to bare soil and urban areas due to the increase of population and urban growth. This is a dangerous threat to Egypt's food security.

REFERENCES

[1]Volpi, M., Tuia, D., Kanevski, M., Bovolo, F. and Bruzzone, L., 2009, September. "**Supervised change detection in VHR images: a comparative analysis**". In *2009 IEEE International Workshop on Machine Learning for Signal Processing* (pp. 1-6). IEEE.

[2]Peng, D. and Zhang, Y., 2017. **Object-based change detection method using refined Markov random field**. Journal of Applied Remote Sensing, 11(1), p.016024.

[3]Lu, D., Mausel, P., Brondízio, E., Moran, E., 2004. "**Change detection techniques**". International Journal of Remote Sensing 25, 2365–2401.

[4]Mostafa, Y., 2006. "**Comparison of Land cover change detection methods using SPOT images**". Master of Science, Department of Civil Engineering, Assiut University, Egypt.

[5]Jianya, G., Haigang, S., Guorui, M. and Qiming, Z., 2008. **"A review of multi-temporal remote sensing data change detection algorithms**". *The International Archives of the Photogrammetry, Remote Sensing and Spatial Information Sciences*, *37*(B7), pp.757-762.

[6]Tewkesbury, A.P., Comber, A.J., Tate, N.J., Lamb, A. and Fisher, P.F., 2015. **A critical synthesis of remotely sensed optical image change detection techniques**. *Remote Sensing of Environment, 160, pp.1-14*.

[7]Coppin, P., Jonckheere, I., Nackaerts, K., Muys, B. and Lambin, E., 2004. **"Digital change detection methods in ecosystem monitoring: a review".** *International journal of remote sensing*, *25*(9), pp.1565-1596.

[8]Chen, Q. and Chen, Y., 2016. "**Multi-feature object-based change detection using self-adaptive weight change vector analysis**". *Remote Sensing*, *8*(7), p.549.

[9]Zhang, Y., Peng, D. and Huang, X., 2018. "**Object-based change detection for VHR images based on multiscale uncertainty analysis**". *IEEE Geoscience and Remote Sensing Letters*, *15*(1), pp.13-17.

[10]Hussain, M., Chen, D., Cheng, A., Wei, H. and Stanley, D., 2013." **Change detection from remotely sensed images: From pixel-based to object-based approaches**". *ISPRS Journal of photogrammetry and remote sensing, 80, pp.91-106.*

[11]Blaschke, T., 2010."**Object based image analysis for remote sensing"**. ISPRS Journal of Photogrammetry and Remote Sensing 65, 2–16.

[12]Chen, G., Hay, G.J., Carvalho, L.M. and Wulder, M.A., 2012. "**Object-based change detection**". *International Journal of Remote Sensing*, *33*(14), pp.4434-4457.

[13]Hong, G. and Zhang, Y., 2008. "**Wavelet-based image registration technique for high-resolution remote sensing images"**. *Computers &Geosciences*, *34*(12), pp.1708-1720.

[14]Mostafa, Y., and A. Abedehafez. 2017a. **Shadow Identification in High Resolution Satellite Images in the Presence of Water Regions**. *Photogrammetric Engineering and Remote Sensing* 83 (2): 87–94

[15]Mostafa, Y., and A. Abedehafez. 2017b. **Accurate Shadow Detection from High-Resolution Satellite Images**. *IEEE Geoscience and Remote Sensing Letters* 14 (4): 494-498.

[16]Mostafa, Y., and M. Abdelwahab. 2018. **Corresponding regions for shadow restoration in satellite high-resolution images**. *International Journal of Remote Sensing* 39 (20): 7014–7028.

[17]Mostafa, Y. 2017. **A Review on Various Shadow Detection and Compensation Techniques in Remote Sensing Images**. *Canadian Journal of Remote Sensing* 43 (6): 545–562.

[18]Hester, D.B., 2008. "**Land Cover Mapping and Change Detection in Urban Watersheds Using QuickBird High Spatial Resolution Satellite Imagery**". Ph.D. Dissertation, Faculty of North Carolina State University.

[19]Johansen, K., Arroyo, L.A., Phinn, S. and Witte, C., 2008." **Object-oriented change detection of riparian environments from high spatial resolution multi-spectral**

images". *Proceedings of the GEOgraphic Object Based Image Analysis for the 21st Century (GEOBIA): Pixels, Objects, Intelligence, Calgary, Canada*, pp.1-6.

[20]Campbell, J., 2002. "**Introduction to Remote Sensing**". Third Edition, London and New York: Taylor & Francis.

[21]Alavi Shoushtari, N., 2012. *"***Land Use and Land Cover Change Detection in Isfahan***"*, *Iran Using Remote Sensing Techniques*(Doctoral dissertation, Université d'Ottawa/University of Ottawa).

[22]Deng, J.S., Wang, K., Deng, Y.H. and Qi, G.J., 2008. **"PCA-based land-use change detection and analysis using multitemporal and multisensor satellite data".** *International Journal of Remote Sensing*, *29*(16), pp.4823-4838.

[23]Farrag, A., and Mostafa, Y., 2006 "**Comparison of Land Cover Change Detection Techniques with Satellite Images: Case Study in Assiut, Egypt**" Civil Engineering Research Magazine, Al-Azhar University, Volume 28, No.(3) , pp. 983- 996.

إكتشاف التغيرات على سطح الارض
باستخدام صور الأقمار الصناعية عالية الدقة: دراسة مقارنة

الملخص العربي:

يعد اكتشاف التغيرات هو أحد التطبيقات الهامة للاستشعار عن بعد, حيث توفر الأقمار الصناعية الحديثة مثل WorldView and GeoEye صور عالية الدقة تساعد في تحسين اكتشاف التغيرات وتحديدها. وفى العقود الأخيرة تم تطوير العديد من الطرق لتحديد التغيرات واكتشافها. الهدف الرئيسي من هذه الدراسة هو إيجاد أفضل طريقة من طرق اكتشاف التغيرات التي يمكن تطبيقها على البيئة المصرية باستخدام صور الأقمار الصناعية عالية الدقة. في هذه الدراسة تم اختبار خمس طرق لاكتشاف التغيرات وهم:

post classification comparison, multi-date direct classification, image differencing, image ratio, and principal component analysis.

وذلك باستخدام صورتان ملتقطتان بواسطة القمر الصناعي WorldView لعام 2016 و القمر الصناعي Ikonos لعام 2006 لمدينة أسيوط وما حولها. في بداية العمل تم تهيئة الصور من خلال عمل تصحيح هندسي لصورة عام 2016 باستخدام صورة عام 2006, ثم تحسين الظل. بعد ذلك تم تطبيق الطرق المختلفة لاكتشاف التغيرات وقياس دقة وفاعلية كلا منها. وقد أظهرت النتائج تفوق طريقة principal component analysis على قريناتها من الطرق. كما وجد أن أعلى نسبة من التغير كانت من مناطق زراعية الي مباني بنسبة (2.86٪). ويرجع ذلك الي زيادة عدد السكان والتوسع في البناء بالتعدي علي الرقعة الزراعية. ويليها التحول من الأراضي الزراعية إلى الأراضي الصحراوية بنسبة (1,46٪) بغرض التوسع العمراني أيضا وكذلك التطور الصناعي على حساب الرقعة الخضراء وأقل نسبة كانت للتحول من الأراضي الصحراوية إلى الأراضي الزراعية بنسبة (0,31٪) وهى نسبة ضئيلة جداً مما يعتبر تهديدا خطيراً لأمن مصر الغذائي في المستقبل.